HHS Public Access

Author manuscript

Adv Funct Mater. Author manuscript; available in PMC 2019 July 19.

Published in final edited form as:

Adv Funct Mater. 2018 September 5; 28(36): . doi:10.1002/adfm.201803417.

Near-Infrared IIb Fluorescence Imaging of Vascular Regeneration with Dynamic Tissue Perfusion Measurement and High Spatial Resolution

Zhuoran Ma,
Department of Chemistry, Stanford University, 380 Roth Way, Stanford, CA 94305-5080

Mingxi Zhang,
Department of Chemistry, Stanford University, 380 Roth Way, Stanford, CA 94305-5080

Jingying Yue,
Department of Chemistry, Stanford University, 380 Roth Way, Stanford, CA 94305-5080

Cynthia Alcazar,
Veterans Affairs Palo Alto Health Care System, 3801 Miranda Avenue, Palo Alto, CA, 94304, USA

Yeteng Zhong,
Department of Chemistry, Stanford University, 380 Roth Way, Stanford, CA 94305-5080

Timothy C. Doyle,
Department of Pediatrics, Stanford University, 318 Campus Drive West Stanford, CA, 94305

Hongjie Dai, and
Department of Chemistry, Stanford University, 380 Roth Way, Stanford, CA 94305-5080, hdai1@stanford.edu

Ngan F. Huang
Department of Cardiothoracic Surgery and Cardiovascular Institute, Stanford University, 300 Pasteur Drive, Stanford, CA 94305-5407, USA, ngantina@stanford.edu

Abstract

Real-time optical imaging is a promising approach for visualizing *in vivo* hemodynamics and vascular structure in mice with experimentally induced peripheral arterial disease (PAD). We report the application of a novel fluorescence-based all-optical imaging approach in the near-infrared IIb (NIR-IIb, 1500–1700 nm emission) window, for imaging hindlimb microvasculature and blood perfusion in a mouse model of PAD. In phantom studies, lead sulfide/cadmium sulfide (PbS/CdS) quantum dots showed better retention of image clarity, in comparison with single-walled nanotube (SWNT) NIR-IIa (1000–1400nm) dye, at varying depths of penetration. When systemically injected to mice, PbS/CdS demonstrated improved clarity of the vasculature, compared to SWNTs, as well as higher spatial resolution than *in vivo* microscopic computed

Supporting Information
Supporting Information is available from the Wiley Online Library or from the author.

Conflict of Interest.
The authors declare no conflict of interest.

tomography. In a mouse model of PAD, NIR-IIb imaging of the ischemic hindlimb vasculature showed significant improvement in blood perfusion over the course of 10 days ($P<0.05$), as well as a significant increase in microvascular density over the first 7 days after induction of PAD. In conclusion, NIR-IIb imaging of PbS/CdS vascular contrast agent is a useful multi-functional imaging approach for high spatial resolution imaging of the microvasculature and quantification of blood perfusion recovery.

Graphical Abstract

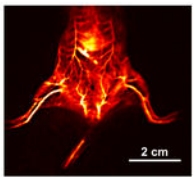

Keywords

quantum dots; fluorescence imaging; peripheral arterial disease

1. Introduction

Fluorescence imaging is a promising approach for real-time visualization of *in vivo* hemodynamics and vascular structure. Compared to fluorescence imaging in the visible and near-infrared wavelengths (<900 nm), imaging in the second near-infrared window (NIR-II, 1000–1700 nm) allows for deep-tissue and high-resolution, owing to large fluorophore Stokes shifts and reduced scattering of photons traversing biological tissues.[1–3] Various kinds of NIR-II agents have been reported by us and others, including polymers,[4–7] small molecular dyes,[8–11] quantum dots,[12–15] rare-earth nanocrystals,[16–19] and single walled nanotubes (SWNTs).[20–23] Within the NIR-II window, agents in the long end of the NIR-II window (named the NIR-IIb optical window, 1500–1700nm) are characterized by greater spatial resolution and deeper penetration depth, than when compared to agents that fluoresce in the NIR-IIa optical window (1100–1400 nm), along with nearly zero endogenous tissue autofluorescence.

A clinically relevant application of NIR-II imaging is for imaging of the vasculature in ischemic tissue in which there is reduced blood flow. In particular, peripheral arterial disease (PAD) is characterized by the narrowing of the arteries that supply blood flow to the limbs, and affects over 10 million people in the United States.[24] Patients with a severe form of PAD have critical limb ischemia and are at risk of limb amputation. Biological approaches to treat PAD, including cell or protein therapies have shown only moderate benefit in late-phase clinical trials.[25–27] Accordingly, there is a great demand for new biological or pharmacological therapies that can improve vascular generation and restore blood perfusion

to the site of limb ischemia. Experimental therapies to treat PAD are frequently tested in a murine model of PAD.[28] Therefore, the ability to employ NIR-II vascular contrast agents to evaluate the efficacy of experimental therapies based on non-invasive hemodynamic and anatomical information would be beneficial.

Previously, we reported the application of SWNTs that are intrinsically fluorescent in the NIR-IIa optical window.[20, 21] When injected intravenously into mice as a blood contrast dye, coupled with real-time video acquisition, the SWNTs served as a multi-functional dye that achieved higher spatial resolution in vascular architecture when compared to conventional microscopic computed tomography (μCT), while matching the temporal resolution of blood flow quantification using ultrasonography.[20] NIR-IIa imaging of SWNTs in ischemic hindlimbs led to quantitative assessment of blood perfusion recovery.[21]

We recently developed molecular imaging agents derived from the NIR-IIb optical window (1500–1700nm).[17, 29] Here, we apply the use of a NIR-IIb agent, lead sulfide/cadmium sulfide (PbS/CdS)[30, 31], as a vascular contrast agent for imaging of the murine hindlimb vasculature in normal and ischemic conditions. We show that the NIR-IIb vascular contrast dye shows superior fluorescence imaging clarity and resolution compared to the SWNT NIR-IIa contrast agent, along with improved image resolution compared to μCT. As a multi-functional dye, PbS/CdS further provides dynamic quantification of blood flow and blood perfusion over the course of recovery from hindlimb ischemia.

2. Results and Discussion

2.1. Comparison of NIR-II Fluorescence imaging using SWNTs and PbS/CdS in Tissue Phantoms

Compared to conventional NIR-I (700–900 nm) and NIR-II (1000–1700 nm) windows, fluorescence imaging in the NIR-IIb window (1500–1700 nm) benefits from significantly reduced tissue scattering and autofluorescence, which could afford higher spatial resolution and deeper tissue penetration. In this study, PbS/CdS was used as a NIR-IIb contrast dye due to its longer emission wavelength and higher quantum yield, compared to previously reported values for SWNTs,[32, 33] which makes it suitable for deep tissue imaging with higher spatial and temporal resolution. PbS/CdS core/shell quantum dots were prepared according to reported methods.[34, 35] The surface was modified by a mixture of mPEG-NH2 (M.W. = 5 k) and 8-arm PEG-NH2 (M.W. = 40 k) to increase the biocompatibility (Figure 1A). As prepared, PbS/CdS quantum dots had a high quantum yield of ~2% - 20% (using quantum yield of IR26 = 0.05% - 0.5% in DCE as a reference) with an emission peak at ~1600 nm (Figure 1B) and endogenous autofluorescence in the NIR-IIb window (Figure 1C). The mean size of the quantum dots was 6.8 ± 0.3 nm (Figure S1), based on transmission electron microscopy (TEM). Next, a tissue phantom study using Intralipid (1 wt% aqueous solution) that mimics the optical properties of biological tissues was performed to compare the clarity and penetration depth of PbS/CdS and with NIR-IIa contrast agent, SWNTs (Figure 1D). The reduced scattering coefficient of Intralipid is inversely proportional to wavelength ($\mu_s' = 1.6\lambda^{-2.4}$, where μ_s' is the reduced scattering coefficient (in mm^{-1}) and λ is the wavelength (in μm)). Capillary tubes filled with PbS/CdS

or SWNTs were immersed at different depths. When the capillary tubes were close to the surface (depth = 0 or 2 mm), a sharp image could be formed in both NIR-IIa and NIR-IIb windows (Figure 1D). However, the measured size of the capillary tube was significantly broadened with the increase of depth in the NIR-II window. In contrast, a sharp image could be maintained in the NIR-IIb window at a penetration depth of 6 mm (Figure 1E) due to largely reduced scattering. The phantom study indicated that using PbS/CdS as a NIR-II contrast dye could afford better spatial resolution at deeper tissue penetration.

2.2 NIR-IIa and NIR-IIb Fluorescence Imaging of Murine Hindlimb Vasculature

Since SWNT has been used previously as a NIR-IIa contrast dye for imaging of mouse hindlimb vasculatures, we next compared the imaging clarity and spatial resolution of the two contrast dyes, SWNTs (200 μL, 0.1 mg/mL) and PbS/CdS (200 μL, 5 mg/mL) by sequential injection into the same mice. The image was recorded using a liquid nitrogen-cooled 2D InGaAs camera with different emission filters, and an adjustable lens set was used to afford different magnification. When SWNT was used as a contrast agent, there was a high background signal due to tissue scattering and autofluorescence. In contrast, when the same mouse was imaged in the NIR-IIb window using PbS/CdS as a contrast agent, there was a significantly improved spatial resolution and signal-to-background ratio at all magnifications (Figure 2A-F). The vessel structure could be clearly identified at the whole-body level (Figure 2B) or at the hindlimb level (Figure 2F). To confirm that the fluorescence intensity was derived from PbS/CdS quantum dots and not from SWNTs, we demonstrated that SWNTs had no fluorescent signal in the NIR-IIb window (Figure S2).

Using movies capturing NIR-IIa and NIR-IIb fluorescence within the vasculature upon tail vein injection, principal component analysis (PCA) was performed to differentiate arteries and veins. When SWNTs or PbS/CdS was injected intravenously into a mouse, the fluorescence signal from the femoral artery was first observed, followed by the signal from the femoral vein. By grouping pixels with similar time variance behavior into different component, femoral artery could be differentiated from the venous vessels. The PCA for SWNTs and PbS/CdS showed similar assignment results for the same vessel, indicating PbS/CdS could also be used to identify arteries and veins.

Fluorescence imaging at higher magnification was next performed to visualize smaller, higher-order branches of blood vessels (Figure 2E,F). The diameter of the vessels was measured by calculating the Gaussian-fitted full width at half maximum (FWHM) of the cross-sectional fluorescence intensity profile (Figure 2G,H). Compared to PbS/CdS, SWNTs generally showed a ~1.5–2 fold broadening of the same vessel structure, which could be attribute to stronger scattering of photons at lower wavelength. Consequently, the size of the vessels could be more accurately determined by using PbS/CdS as a contrast agent.

2.3 Comparison of Murine Hindlimb Vascular Imaging between NIR-IIb and μCT

We next compared the quality of the murine hindlimb vasculature by NIR-IIb imaging of PbS/CdS contrast dye to μCT imaging. The resulting μCT images reflect a 3D volume rendering that display the contrast-enhanced regions of the animal (ie, the vasculature) as well as the skeletal structures. By sequentially imaging the same mice using both imaging

techniques at a similar voxel size, a side-by-side comparison could be made. As shown in Figure 3A,B, NIR-IIb imaging showed superior visualization of microvasculature below the knee, compared to μCT imaging. Furthermore, the number and width of vessels were quantified by image analysis, in which the intensity values that intersect the line perpendicular to the femoral vessels were measured (Figure 3C,D). The histograms showing intensity versus physical location were used to identify vessels represented by individual peaks based on either NIR-IIb or μCT images. Based on image analysis, NIR-IIb imaging could detect 5 times greater number of hindlimb vessels, compared to μCT imaging (51±2 vessels NIR-IIb vs 11±2 vessels μCT) (Figure 3E). Furthermore, NIR-IIb could resolve more small vessels (<100μm diameter) than μCT imaging (Figure 3F). These data suggested that NIR-IIb was able to a greater number of small vessels, compared to μCT imaging.

A variety of imaging modalities, including laser Doppler spectroscopy, magnetic resonance imaging, and μCT have been used for dynamic vascular perfusion measurement or vascular structural imaging.[36–39] In comparison, NIR-IIb fluorescence imaging has shown high spatial and temporal resolution like μCT with dynamic perfusion measurements like laser Doppler spectroscopy. Different kinds of NIR-II fluorophores have been developed for *in vivo* imaging, including SWNTs, quantum dots, rare-earth nanoparticles, conjugated copolymers and organic small-molecule fluorophores.[8, 17, 21, 40, 41] These fluorophores have been utilized for visualizing cerebral or hindlimb vasculatures, targeting tumors, and mapping lymph nodes.[17, 20, 42–44] However, most NIR-II fluorophores emit at the NIR-IIa (1000–1400 nm) window, which limits tissue penetration and spatial resolution. In comparison to NIR-IIa fluorophores, PbS/CdS quantum dots have longer emission wavelength and higher quantum yield in aqueous solution, which makes it suitable for deep tissue imaging with higher spatial and temporal resolution.

2.4 NIR-IIb Imaging of Blood perfusion Recovery in Ischemic hindlimb

To apply NIR-IIb imaging for vascular perfusion recovery in the setting of PAD, we induced unilateral hindlimb ischemia by ligation and excision of the femoral artery. At time points between 0–10 days after induction of ischemia, the mice were evaluated for tissue perfusion based on NIR-IIb imaging, in comparison to conventional laser Doppler spectroscopy (Figure 4A-D).

Similar to laser Doppler spectroscopy, NIR-IIb fluorescence–based dynamic perfusion imaging revealed a steady and statistically significant ($P<0.05$) recovery of blood perfusion to the ischemic hindlimb from day 0 to day 10 after surgery (Figure 4E), with both perfusion quantification approaches reaching greater than 80% perfusion on day 10 post-surgery. However, in comparison to laser Doppler images, those derived from NIR-IIb fluorescence imaging afforded higher spatial resolution and discrimination of vascular structures in the hindlimb, resembling that of angiograms (Figure 4A,B).

Based on real-time video acquisition of PbS/CdS movement within the vasculature of the hindlimbs (Video 1 & Video 2), blood flow to the ischemic limb could be quantified as a function of time (Figure 4F). The calculated absolute blood flow rate of the ischemic limb exhibited a statistically significant increase ($P < 0.05$) as a function of time post hindlimb ischemia from day 0 to day 10. Consistent with previous studies that have shown little

toxicity of SWNTs or PbS/CdS at such concentration *in vivo*, [45–47] we detected no evidence of acute toxicity based on histological analysis of spleen and liver samples within 24h after contrast agent injection (data not shown). These findings demonstrated the multi-functional ability of NIR-IIb imaging to provide structural information of vascular structure similar to μCT imaging, while providing blood perfusion quantification similar to that of laser Doppler spectroscopy.

2.5 Structural Imaging of Vascular Regeneration in Ischemic Hindlimb

NIR-IIb imaging at higher magnification was then performed to analyze the change of vasculature anatomy in response to hindlimb ischemia (Figure 5A). Compared to the vasculature on day 0, large number of regenerated vessels could be visualized on the ischemic hindlimb in response to the surgical excision of the femoral artery on day 7. In contrast, the vasculature structure of the control (un-operated) limb remained unchanged.

Besides providing information about tissue perfusion, NIR-IIb fluorescence imaging was used to quantify the microvascular density in the ischemic hindlimb. The number of microvessels of the control and ischemic limb was counted manually, and the relative microvasculature density (ischemic/control) was plotted as a function of time (Figure 5B). The results showed a statistically significant increase ($P < 0.05$) of microvascular density of the ischemic limb at day 7 post hindlimb ischemia, followed by a return to normal vessel numbers at day 10, consistent with previously reported results.[21] The results were further confirmed by using an automatic fast Fourier transform (FFT) method of counting vessel numbers (Figure S3). The transient enhancement in microvascular density is likely attributed to acute remodeling in response to tissue ischemia by the initial recruitment of collateral vessels, followed by their gradual regression with tissue remodeling. Together, these data demonstrate the ability of NIR-IIb imaging to visualize vascular regeneration and quantify blood perfusion recovery in a mouse model of PAD.

Although NIR-IIb imaging using PbS/CdS quantum dots as the contrast agent showed great promise for imaging vessel regeneration, there are still some limitations of this method that needs to be considered. First, although NIR-IIb imaging is at least comparable to μCT with respect to spatial resolution, it currently lacks sufficient depth of penetration that is required for clinical translation. As new contrast dye agents evolve with time, the penetration depth will likely become less of a concern. Another potential concern is the toxicity of the quantum dots. Although PbS/CdS quantum dots did not show acute *in vivo* toxicity in this study, the long-term toxicity of the material needs to be assessed more carefully. Developing NIR-IIb-emitting small-molecule fluorophores with low toxicity would facilitate clinical translation of NIR-IIb imaging. In addition, the spatial and temporal resolution of the fluorescence images is limited by the pixel size and the frame rate of the InGaAs camera used. With the development of new near infrared detection techniques, a diffraction-limited spatial resolution (< 1 μm) and an ultrafast frame rate (>60 frames per second) can be achievable. Despite these limitations, the benefits of NIR-IIb imaging will likely lead to more widespread use of this technology for cardiovascular imaging.

3. Conclusion

In conclusion, the salient finding of this study is that: 1) NIR-IIb fluorescence imaging using PbS/CdS contrast agent enables dynamic tissue perfusion measurement and high-resolution structural vascular imaging in a mouse model of PAD; 2) This multifunctional non-invasive imaging approach; combines the function of laser Doppler spectroscopy and vessel imaging quality of μCT imaging into a single modality; 3) Compared to our previously characterized SWNT NIR-IIa contrast agent, PbS/CdS showed superior imaging quality and clarity of vascular structures; and 4) Using NIR-IIb imaging of PbS/CdS, the recovery of limb perfusion after the induction of hindlimb ischemia could be quantitatively assessed for tissue perfusion and microvascular density simultaneously. Consequently, this approach is an attractive non-invasive approach for obtaining multi-functional data using a single imaging modality.

4. Experimental Section

Synthesis of PbS/CdS NIR-IIb Vascular Contrast Agent:

PbS/CdS was synthesized using a modified procedure described previously.[34,35] Briefly, monodispersed PbS quantum dots were first synthesized by a hot-injection method. A CdS layer was then coated on the surface of as-prepared PbS through cation exchange. To further increase its water solubility and biocompatibility, the carboxylic acid groups on the surface of the quantum dots were polyethylene glycol-modified (PEGylated) with mPEG-NH_2 (5 kDa, Laysan Bio) and 8-arm-PEG-NH_2 (40 kDa, Advanced BioChemicals).

Preparation of SWNT NIR-IIa Vascular Contrast Agent:

Biocompatible SWNTs with NIR-II emission of 1100–1400 nm were prepared using a surfactant exchange method according to previous publications.[1, 20, 21,48] Briefly, raw high pressure carbon monoxide conversion SWNTs (Unidym) were suspended in a solution of 1 wt% sodium cholate by bath sonication for 1 hour. The solution was centrifuged at 300, 000 g for 1 hour to remove large bundles. The supernatant was mixed with DSPE-mPEG (1,20distearoyl-sn-glycero-3-phosphoethanolamine-N-[methoxy (polyethylene glycol) 5000]) at a concentration of 1 mg/mL, and dialyzed against PBS with a 3500 Da membrane (Fisher) to remove sodium cholate. As-prepared SWNTs were centrifuged again at $3\times10^5 g$ for 1 hour to remove aggregates. TEM imaging, as described previously,[35] was performed to image the size of the quantum dots.

Measurement of PbS/CdS Fluorescence Emission Spectrum:

The NIR-IIb fluorescence emission spectrum of PbS/CdS was measured by a home-built NIR-II spectrometer. The excitation source was an 808 nm fiber-coupled diode laser (RMPC lasers). The excitation light was filter by selected short-pass filters, and passed through a 1-cm path quartz cuvette filled with PbS/CdS solution. The emission light was filtered by a 900-nm long-pass filter (Thorlabs) and directed into a spectrometer (Acton SP2300i) equipped with an InGaAs linear array detector (Princeton OMA-V). The raw data was corrected according to the sensitivity of the detector and the absorbance features of the emission filter.

Penetration Depth of PbS/CdS in Tissue Phantom:

The penetration depth of PbS/CdS was compared to SWNTs using an absorbing and scattering medium (Intralipid®), as described previously.[1] Glass capillary tubes were filled with either SWNTs (0.01 mg/mL) or PbS/CdS (0.5 mg/mL) and taped to the bottom of a cylindrical dish. The dish was filled with different volumes of 1% Intralipid® (Fresenius Kabi) that approximates the wavelength dependence of light scattering in biological tissues.[49–51] The depth of the capillary tubes was calculated from the area of the dish. The capillary tubes were excited by an 808 nm fiber-coupled diode laser (RMPC lasers) at a power density of 140 mW/cm^2. The excitation light was collimated and filtered by an 850-nm short-pass (Thorlabs) and a 1000-nm short-pass (Thorlabs) filter. The emission light was allowed to pass through emission filters (900-nm long-pass and 1100-nm long-pass for SWNTs, 1100-nm long-pass and 1500-nm long-pass for PbS/CdS) and was collected by a two-dimensional, liquid-nitrogen-cooled InGaAs array with 319×256 pixels.

Comparison of PbS/CdS and SWNT for Fluorescence Imaging of Mouse Hindlimb:

All animal procedures were approved by the Administrative Panel on Laboratory Animal Care at Stanford University. To first compare the imaging clarity of SWNTs and PbS/CdS *in vivo* by NIR-II fluorescence imaging, each healthy C57/BL6 mice (male, 8 weeks old, Charles River) was mounted on a stage beneath an 808 nm diode laser (RMPC lasers). The excitation light was collimated and filtered by an 850-nm short-pass (Thorlabs) and a 1000-nm short-pass (Thorlabs) filter, and the power density was 140 mW/cm^2. The emission light from the mouse was filtered through emission filters (900-nm long-pass and 1100-nm long-pass for SWNTs, 1100-nm long-pass and 1500-nm long-pass for PbS/CdS) and was collected by a two-dimensional, liquid-nitrogen-cooled InGaAs array with 319×256 pixels. Different lens sets were used to obtain tunable magnifications from 1× to 10×. An imaging setup with 1× magnification was used for video-rate imaging. The two-dimensional InGaAs array was set to expose continuously, and fluorescence images were obtained by Labview software. The camera started recording immediately after a 200-μL solution of SWNTs (0.1 mg/mL) was injected into the mouse tail vein. The exposure time was 100 ms, and the frame rate was 5.3 frames/second, due to the overhead time for the acquisition of each frame. To perform hindlimb vascular imaging, the mouse was imaged ≈ 60 minutes after injection using a setup with 10× magnification. For direct comparison of vascular imaging clarity, the same mouse was then allowed to recover before being injected with a 200-μL solution of PbS/CdS (5 mg/mL). Video-rate imaging and vessel structural imaging were then performed using a setup with 1× and 10× magnification, respectively (n = 5). The imaging method was similar to the one used for SWNTs, except that the exposure time of video-rate imaging was 20 ms.

Vessel Structural Imaging Using NIR-II Fluorescence Imaging of PbS/CdS:

An imaging setup with 10× magnification was used for vessel structural imaging, and the pixel size was 28 μm. The mice were imaged at ≈60 minutes after injection. For vessel width analysis, the NIR-II image obtained by the camera was loaded into an array using MATLAB software. A line was drawn perpendicular to the vessel of interest, and the intensity of each

pixel on the line was extracted. The line profile was fitted using a Gaussian function, and the full width at half maximum of the peak was the width of the vessel.

To analyze relative vessel density, vessels of the control or ischemic hindlimb was counted one by one, as described previously.[21] Duplication in vessels counted, such as branches of a larger vessel, was subtracted from the total number of vessels. The total number of vessels of the ischemic limb was normalized against that of the control limb to give relative microvascular density (n=5). A second method using fast Fourier transformation (FFT), as described in previous publications,[21] was used to further validate the results. A Fourier bandpass filter for vessel width between 28 μm and 224 μm was applied to an image of the mouse hindlimb. The filtered frequency domain plot of the ischemic limb was integrated and normalized against the corresponding value of the control limb to obtain the relative vessel density.

Comparison of Vessel Structures between NIR-IIb and μCT Imaging:

For comparison to that of NIR-IIb imaging, vessel structural imaging of normal mice was performed using a μCT scanner (Skyscan 1276, Bruker). In the anesthetized state, the mice were injected with AuroVist 15nm gold nanoparticles (Nanoprobes) contrast agent (12 mg Au in 0.2ml PBS) into the tail vein. The contrast agent was injected slowly into the tail vein of the mice during 30 to 60 s to prevent embolization. The μCT scans were acquired within 30 minutes after injection. The animals were placed in prone position in the scanner and anesthetized with 2% isoflurane with a 1-L/min O2 flow rate. Each scan was acquired using the settings of 70 kV, 200 μAmps with 0.5 mm aluminum filtration, 0.8° step size, detector binning 4×4 and 450 views (2 frames average, 158msec/frame exposure) per animal (total scan time ~7 minutes). After acquisition of contrast-enhanced μCT images, three-dimensional reconstruction to a 32-μm isotopic voxel size was performed using NRecon software and the InstaRecon processing interface, and reconstructed data was imported into Amira 5.6 for visualization. The images had no perspective applied to them such that the depth dimension is the same as the x-y scales shown on the image. For vessel width analysis, a line was drawn on each μCT image, perpendicular to the vessels of interest, while avoiding the bone features. Then the contrast profile was analyzed in a manner similar to NIR-II images to obtain vessel widths (n=3). Where specified, animals were euthanized within 24h after PbS/CdS dye injection for cryosectioning and subsequent hematoxylin and eosin staining of tissue sections for analysis of acute toxicity.

NIR-IIb Imaging of Blood Perfusion in the Ischemic Hindlimb Using PbS/CdS Contrast Agent:

Male C57/BL6 mice were anesthetized and maintained under 2% isoflurane and oxygen flow rate of 1 L/min. In the anesthetized state, unilateral hind limb ischemia was induced by ligation and excision of the left femoral artery, as previously reported.[37,52] The right limb served as the non-ischemic control. NIR-IIb imaging was performed on ischemic hind limbs using PbS/CdS contrast dye using the same protocol for healthy hindlimbs described above. The time points of NIR-II imaging (days 0, 3, 7, and 10) referred to the number of days after induction of hindlimb ischemia (n>4 per time point). NIR-IIb fluorescence-based blood perfusion measurement was performed based on methods described in previous publications.

[20, 21] An imaging setup with 1× magnification was used. For video-rate imaging, a mouse was mounted on the stage in its supine position before injection. To calculate the relative blood perfusion, imaging frames from t = 0 to t = 60 seconds post-injection were loaded into an array using MATLAB software. The same regions of interest of both control and ischemic limbs were selected from the imaging frames, and the average fluorescence intensity was plotted as a function of time. The fluorescence intensity increased linearly before reaching a plateau. The fluorescence signal was normalized against the saturation level of the control hindlimb. A linear fit was performed on the rising edge of the normalized curve, and the slop represented the blood perfusion level of the hindlimb. The slope of the ischemic limb was then normalized against the slope of the control limb to obtain the relative blood perfusion.

To calculate the absolute blood flow velocity of the hindlimb, the position of the front of the fluorescence signal was extracted from each frame, and plotted as a function of time, as described previously.[20] In early frames, the distance travelled by blood front showed a linear increase versus time, and the slope of the linear fit was the speed of the blood flow.

Blood Perfusion Measurement by Laser Doppler Spectroscopy:

To validate blood perfusion quantification of mouse hindlimb using PbS/CdS contrast dye, we further quantified blood perfusion using conventional laser Doppler spectroscopy (PIM3, Permed AB).[21, 28] The animals with induced hindlimb ischemia were anesthetized and maintained under 2% isoflurane and oxygen flow rate of 1 L/min. Hair was removed from both hindlimbs using a depilatory cream and then prewarmed to 37°C body temperature using a heating plate. In the supine position, laser Doppler blood spectroscopy was performed on both hindlimbs. Blood perfusion recovery over time was expressed as the relative ratio of perfusion in the ischemic over the non-ischemic limb ($n<4$).

Statistical Analysis:

Data are expressed as mean ± standard deviation. For comparison of blood perfusion at multiple time points, a repeated measure analysis of variance (ANOVA) with Bonferroni post-test was used. Statistical analysis was performed using Graphpad Prism 6.0. Statistical significance was accepted at $p < 0.05$.

Supplementary Material

Refer to Web version on PubMed Central for supplementary material.

Acknowledgements

Z.M. and M.Z. contributed equally to this work. This study was supported by grants from the US National Institutes of Health to NFH (R00 HL098688, R01 HL127113, R01HL142718, and R21 EB020235), HD (DP1-NS-105737) and TD (1S10OD02349701), and a Merit Review Award (1I01BX002310) to NFH from the Department of Veterans Affairs Biomedical Laboratory Research and Development.

References

[1]. Welsher K, Sherlock SP, Dai H, Proc. Natl. Acad. Sci. U. S. A 2011, 108,8943. [PubMed: 21576494]

[2]. Hong G, Diao S, Chang J, Antaris AL, Chen C, Zhang B, Zhao S, Atochin DN, Huang PL, Andreasson KI, Kuo CJ, Dai H, Nat. Photonics 2014, 8,723. [PubMed: 27642366]

[3]. Zhang Y, Hong G, Zhang Y, Chen G, Li F, Dai H, Wang Q, ACS Nano. 2012, 6,3695. [PubMed: 22515909]

[4]. Tao Z, Hong G, Shinji C, Chen C, Diao S, Antaris AL, Zhang B, Zou Y, Dai H, Angew. Chem. Int. Ed. Engl 2013, 52,13002. [PubMed: 24174264]

[5]. Prosposito P, Casalboni M, De Matteis F, Glasbeek M, Quatela A, van Veldhoven E, Zhang H, J. Lumin 2001, 94,641.

[6]. Kamimura M, Takahiro S, Yoshida M, Hashimoto Y, Fukushima R, Soga K, Polym. J 2017, 49,799.

[7]. Shou KQ, Tang YF, Chen H, Chen S, Zhang L, Zhang A, Fan QL, Yu AX, Cheng Z, Chem. Sci 2018, 9,3105. [PubMed: 29732093]

[8]. Antaris AL, Chen H, Cheng K, Sun Y, Hong G, Qu C, Diao S, Deng Z, Hu X, Zhang B, Zhang X, Yaghi OK, Alamparambil ZR, Hong X, Cheng Z, Dai H, Nat. Mater 2016, 15,235. [PubMed: 26595119]

[9]. Sun Y, Ding MM, Zeng XD, Xiao YL, Wu HP, Zhou H, Ding BB, Qu CR, Hou W, Er-bu AGA, Zhang YJ, Cheng Z, Hong XC, Chem. Sci 2017, 8,3489 [PubMed: 28507722]

[10]. Cosco ED, Caram JR, Bruns OT, Franke D, Day RA, Farr EP, Bawendi MG, Sletten EM, Angew. Chem. Int. Ed. Engl 2017, 56,13126. [PubMed: 28806473]

[11]. Li B, Lu L, Zhao M, Lei Z, Zhang F, Angew. Chem. Int. Ed. Engl 2018, DOI:10.1002/anie.201801226.

[12]. Franke D, Harris DK, Chen O, Bruns OT, Carr JA, Wilson MW, Bawendi MG, Nat. Commun 2016, 7,12749. [PubMed: 27834371]

[13]. Tsukasaki Y, Morimatsu M, Nishimura G, Sakata T, Yasuda H, Komatsuzaki A, Watanabe TM, Jin T, Rsc Adv 2014, 4,41164.

[14]. Chen GC, Tian F, Zhang Y, Zhang YJ, Li CY, Wang QB, Adv. Funct. Mater 2014, 24,2481.

[15]. Zebibula A, Alifu N, Xia LQ, Sun CW, Yu XM, Xue DW, Liu LW, Li GH, Qian J, Adv. Funct. Mater 2018, 28,1703451.

[16]. Naczynski DJ, Tan MC, Zevon M, Wall B, Kohl J, Kulesa A, Chen S, Roth CM, Riman RE, Moghe PV, Nat. Commun 2013, 4,2199. [PubMed: 23873342]

[17]. Zhong Y, Ma Z, Zhu S, Yue J, Zhang M, Antaris AL, Yuan J, Cui R, Wan H, Zhou Y, Wang W, Huang NF, Luo J, Hu Z, Dai H, Nat. Commun 2017, 8,737. [PubMed: 28963467]

[18]. Villa I, Vedda A, Cantarelli IX, Pedroni M, Piccinelli F, Bettinelli M, Speghini A, Quintanilla M, Vetrone F, Rocha U, Jacinto C, Carrasco E, Rodriguez FS, Juarranz A, del Rosal B, Ortgies DH, Gonzalez PH, Sole JG, Garcia DJ, Nano Res. 2015, 8,649.

[19]. Naczynski DJ, Sun C, Turkcan S, Jenkins C, Koh AL, Ikeda D, Pratx G, Xing L, Nano Lett. 2015, 15,96. [PubMed: 25485705]

[20]. Hong G, Lee JC, Robinson JT, Raaz U, Xie L, Huang NF, Cooke JP, Dai H, Nat. Med 2012, 18,1841. [PubMed: 23160236]

[21]. Hong G, Lee JC, Jha A, Diao S, Nakayama KH, Hou L, Doyle TC, Robinson JT, Antaris AL, Dai H, Cooke JP, Huang NF, Circ. Cardiovasc. Imaging 2014, 7,517. [PubMed: 24657826]

[22]. Yi HJ, Ghosh D, Ham MH, Qi JF, Barone PW, Strano MS, Belcher AM, Nano Lett. 2012, 12,1176. [PubMed: 22268625]

[23]. Roxbury D, Jena PV, Williams RM, Enyedi B, Niethammer P, Marcet S, Verhaegen M, Blais-Ouellette S, Heller DA, Sci. Rep 2015, 5,14167. [PubMed: 26387482]

[24]. Mozaffarian D, Benjamin EJ, Go AS, Arnett DK, Blaha MJ, Cushman M, de Ferranti S, Despres JP, Fullerton HJ, Howard VJ, Huffman MD, Judd SE, Kissela BM, Lackland DT, Lichtman JH, Lisabeth LD, Liu S, Mackey RH, Matchar DB, McGuire DK, Mohler ER 3rd, Moy CS, Muntner P, Mussolino ME, Nasir K, Neumar RW, Nichol G, Palaniappan L, Pandey DK, Reeves MJ, Rodriguez CJ, Sorlie PD, Stein J, Towfighi A, Turan TN, Virani SS, Willey JZ, Woo D, Yeh RW, Turner MB. C American Heart Association Statistics, S Stroke Statistics, Circulation 2015, 131,e29. [PubMed: 25520374]

[25]. Perin EC, Murphy MP, March KL, Bolli R, Loughran J, Yang PC, Leeper NJ, Dalman RL, Alexander J, Henry TD, Traverse JH, Pepine CJ, Anderson RD, Berceli S, Willerson JT, Muthupillai R, Gahremanpour A, Raveendran G, Velasquez O, Hare JM, Hernandez Schulman I, Kasi VS, Hiatt WR, Ambale-Venkatesh B, Lima JA, Taylor DA, Resende M, Gee AP, Durett AG, Bloom J, Richman S, G'Sell P, Williams S, Khan F, Gyang Ross E, Santoso MR, Goldman J, Leach D, Handberg E, Cheong B, Piece N, DiFede D, Bruhn-Ding B, Caldwell E, Bettencourt J, Lai D, Piller L, Simpson L, Cohen M, Sayre SL, Vojvodic RW, Moye L, Ebert RF, Simari RD, Hirsch AT, N Cardiovascular Cell Therapy Research, Circulation 2017, 135,1417. [PubMed: 28209728]

[26]. Raval Z, Losordo DW, Circ. Res 2013, 112,1288. [PubMed: 23620237]

[27]. Annex BH, Nat. Rev. Cardiol 2013, 10,387. [PubMed: 23670612]

[28]. Niiyama H, Huang NF, Rollins MD, Cooke JP, J. Vis. Exp 2009, 23,1035.

[29]. Zhu S, Yang Q, Antaris AL, Yue J, Ma Z, Wang H, Huang W, Wan H, Wang J, Diao S, Zhang B, Li X, Zhong Y, Yu K, Hong G, Luo J, Liang Y, Dai H, Proc. Natl. Acad. Sci. U. S. A 2017, 114,962. [PubMed: 28096386]

[30]. Zhao HG, Wang DF, Zhang T, Chaker M, Ma DL, Chem. Commun 2010, 46,5301.

[31]. Ren F, Zhao H, Vetrone F, Ma D, Nanoscale. 2013, 5,7800. [PubMed: 23887182]

[32]. Jin T, Imamura Y, Ecs J Solid State Sci. Technol 2016, 5,R3138.

[33]. Crochet J, Clemens M, Hertel T, J. Am. Chem. Soc 2007, 129,8058. [PubMed: 17552526]

[34]. Cademartiri L, Bertolotti J, Sapienza R, Wiersma DS, von Freymann G, Ozin GA, J. Phys. Chem. B 2006, 110,671. [PubMed: 16471585]

[35]. Zhang M, Yue J, Cui R, Ma Z, Wan H, Wang F, Zhu S, Zhou Y, Kuang Y, Zhong Y, Pang DW, Dai H, Proc. Natl. Acad. Sci. U. S. A 2018, doi: 10.1073/pnas.1806153115.

[36]. Huang NF, Niiyama H, Peter C, De A, Natkunam Y, Fleissner F, Li Z, Rollins MD, Wu JC, Gambhir SS, Cooke JP, Arterioscler. Thromb. Vasc. Biol 2010, 30,984. [PubMed: 20167654]

[37]. Nakayama KH, Hong G, Lee JC, Patel J, Edwards B, Zaitseva TS, Paukshto MV, Dai H, Cooke JP, Woo YJ, Huang NF, ACS Nano. 2015, 9,6900. [PubMed: 26061869]

[38]. Tirziu D, Moodie KL, Zhuang ZW, Singer K, Helisch A, Dunn JF, Li W, Singh J, Simons M, Circulation. 2005, 112,2501. [PubMed: 16230502]

[39]. Luo Y, Mohning KM, Hradil VP, Wessale JL, Segreti JA, Nuss ME, Wegner CD, Burke SE, Cox BF, J. Magn. Reson. Imaging 2002, 16,277. [PubMed: 12205583]

[40]. Hong G, Robinson JT, Zhang Y, Diao S, Antaris AL, Wang Q, Dai HJ, Angew. Chem. Int. Ed. Engl 2012, 51,9818. [PubMed: 22951900]

[41]. Hong G, Zou Y, Antaris AL, Diao S, Wu D, Cheng K, Zhang X, Chen C, Liu B, He Y, Wu JZ, Yuan J, Zhang B, Tao Z, Fukunaga C, Dai H, Nat. Commun 2014, 5,4206. [PubMed: 24947309]

[42]. Antaris AL, Chen H, Diao S, Ma Z, Zhang Z, Zhu S, Wang J, Lozano AX, Fan Q, Chew L, Zhu M, Cheng K, Hong X, Dai H, Cheng Z, Nat. Commun 2017, 8,15269. [PubMed: 28524850]

[43]. Robinson JT, Hong G, Liang Y, Zhang B, Yaghi OK, Dai H, J. Am. Chem. Soc 2012, 134,10664. [PubMed: 22667448]

[44]. Robinson JT, Welsher K, Tabakman SM, Sherlock SP, Wang HL, Luong R, Dai H, Nano Res. 2010, 3,779. [PubMed: 21804931]

[45]. Schipper ML, Nakayama-Ratchford N, Davis CR, Kam NW, Chu P, Liu Z, Sun X, Dai H, Gambhir SS, Nat. Nanotechnol 2008, 3,216. [PubMed: 18654506]

[46]. Liu Z, Davis C, Cai W, He L, Chen X, Dai H, Proc. Natl. Acad. Sci. U. S. A 2008, 105,1410. [PubMed: 18230737]

[47]. Benayas A, Ren FQ, Carrasco E, Marzal V, del Rosal B, Gonfa BA, Juarranz A, Sanz-Rodriguez F, Jaque D, Garcia-Sole J, Ma DL, Vetrone F, Adv. Funct. Mater 2015, 25,6650.

[48]. Welsher K, Liu Z, Sherlock SP, Robinson JT, Chen Z, Daranciang D, Dai H, Nat. Nanotechnol 2009, 4,773. [PubMed: 19893526]

[49]. Troy TL, Thennadil SN, J. Biomed. Opt 2001, 6,167. [PubMed: 11375726]

[50]. van Staveren HJ, Moes CJ, van Marie J, Prahl SA, van Gemert MJ, Appl. Opt 1991, 30,4507. [PubMed: 20717241]

[51]. Flock ST, Jacques SL, Wilson BC, Star WM, Vangemert MJC, Lasers Surg. Med 1992, 12,510. [PubMed: 1406004]

[52]. Mulyasasmita W, Cai L, Dewi RE, Jha A, Ullmann SD, Luong RH, Huang NF, Heilshorn SC, J Control. Release 2014, 191,71. [PubMed: 24848744]

Lead sulfide/cadmium sulfide (PbS/CdS) quantum dots emitting in the near-infrared IIb (1500–1700 nm) window demonstrate improved image clarity and spatial resolution compared to NIR-IIa (1000–1400 nm) imaging and microscopic computed tomography. PbS/CdS is used as a contrast agent for multi-functional imaging of hemodynamics and vascular structure in a mouse model of peripheral arterial disease (PAD).

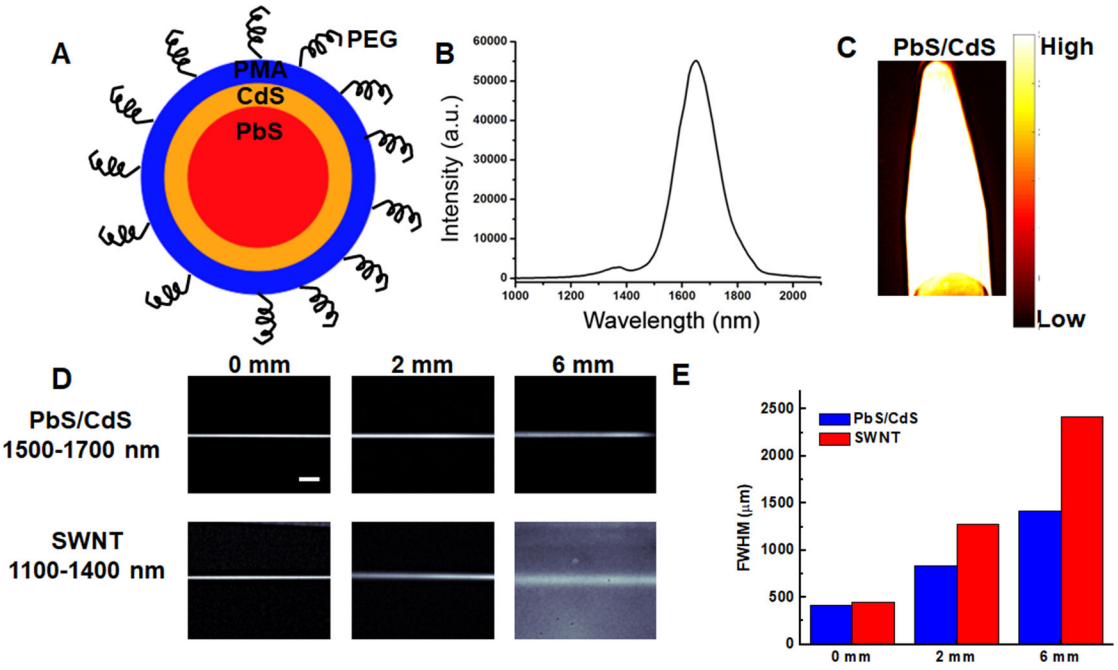

Figure 1.

Comparison of PbS/CdS as a novel blood contrast dye with improved clarity and penetration of depth, compared to SWNTs. A. Schematic diagram showing PbS quantum dot core (red), CdS outer coating (orange), and PMA (blue) with PEG chains on the surface. B. Emission spectrum of PbS/CdS dye showing 1500–1700 nm. C. Fluorescence of PbS/CdS within an eppendorf at 1500–1700 nm emission wavelength. D. Phantom studies comparing the penetration depth of SWNTs (NIR-II) and PbS/CdS (NIR-IIb) at depths of 0, 2, and 6mm in Intralipid® excited at 808 nm. The PbS/CdS sample shows less feature spread than that of the SWNT sample. Scale bar: 5 mm. E. Full width half max (FWHM) measurements depict the feature width of SWNT and PbS/CdS capillary images at varying depths in Intralipid®, showing increased loss of feature integrity for the NIR-II-emitting SWNTs, compared to the NIR-IIb-emitting PbS/CdS.

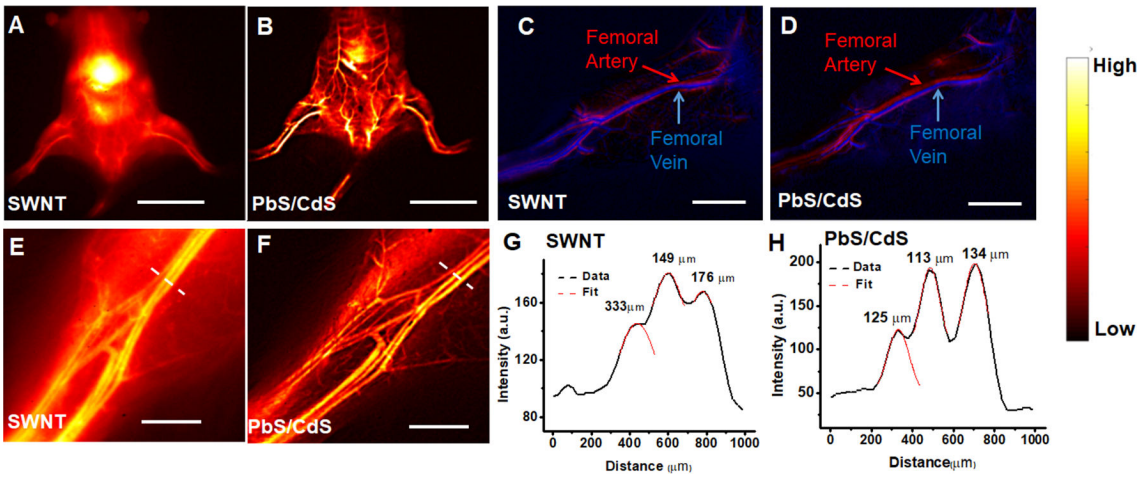

Figure 2.

Comparison of vascular imaging in normal mice using PbS/CdS and SWNT vascular contrast dyes. A,B. Whole body fluorescence imaging of mouse hindlimb vasculature after systemic injection of SWNTs by NIR-II imaging (A), in comparison to NIR-IIb imaging of systemically injected PbS/CdS contrast agent (B). C,D. Principal component analysis of femoral artery and vein after intravenous injection of SWNT (C) or PbS/CdS (D). E,F. High magnification NIR-IIb fluorescence images of the hindlimb vasculature after systemic injection of PbS/CdS (F), in comparison to NIR-II imaging of SWNTs (E). G,H. Representative cross-sectional fluorescence intensity profiles of high magnification images (E,F) along white-dashed bars of a mouse injected with either SWNTs (G) or PbS/CdS (H). Gaussian fits to the profiles are shown in red dashed curves. Scale bar: 2 cm (A,B); 5 mm (C,D), 2 mm (E,F).

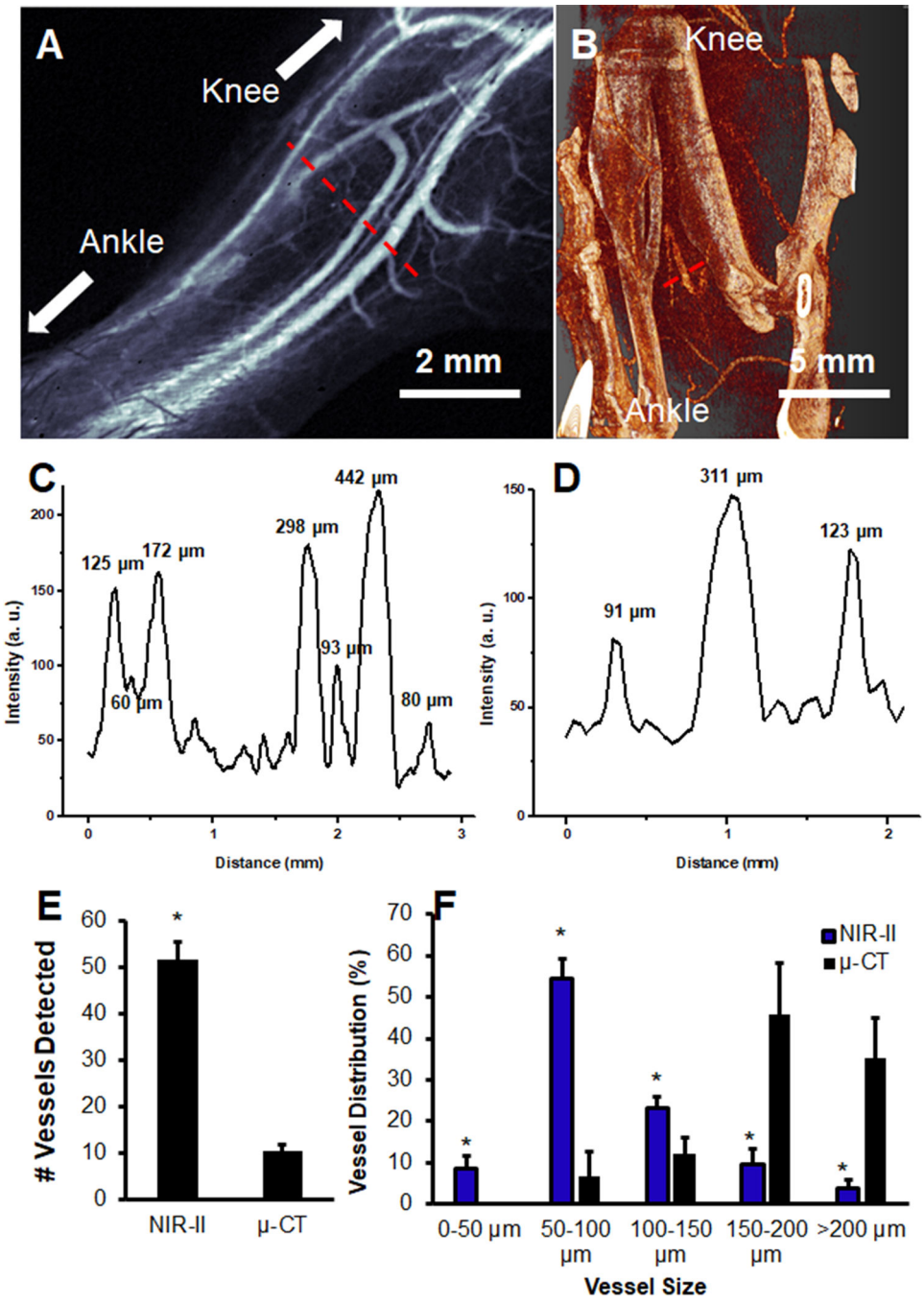

Figure 3.

Comparison of NIR-IIb fluorescence imaging and microscopic computed tomographic (μCT) images of normal mouse hindlimb vasculature. A,B. Comparison of hindlimb vasculature between NIR-IIb (A) and μCT (B). C,D. Representative cross-sectional fluorescence intensity profiles of high magnification images along red bars of a mouse by NIR-IIb imaging (C) or μCT imaging (D). Gaussian fits to the profiles are shown in the histograms (n=3). E,F. Average total vessels (E) and distribution of vessel sizes (F) detected by NIR-IIb and μCT (n=3). Scale bar: 2 mm (A); 5 mm (B).

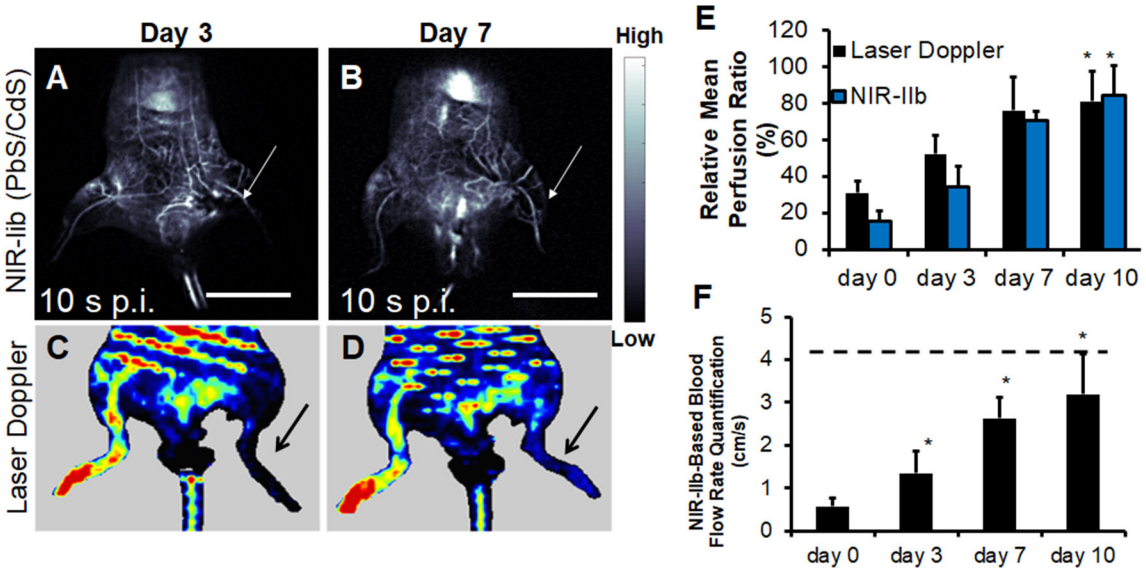

Figure 4.

Quantification of blood perfusion recovery in the ischemic limb by NIR-IIb fluorescence imaging. A-B. NIR-IIb imaging of ischemic hindlimbs mice on days 3 and days 7 using PbS/CdS. Fluorescence images both correspond to the time point of 10 s post-injection (p.i.). C-D. Representative laser Doppler spectroscopy images of ischemic limbs on days 3 and 7, respectively. E. Comparison of relative mean blood perfusion recovery in the ischemic limb by laser Doppler spectroscopy and NIR-IIb fluorescence imaging (n>4). F. NIR-IIb-based quantification of blood flow rate. Dotted line denotes mean flow rate of control non-ischemic limb (n>4). F. Scale bar: 2 cm. Arrow points to ischemic limb. Scale bar: 2 cm (A,B). * $P<0.05$, compared to day 0.

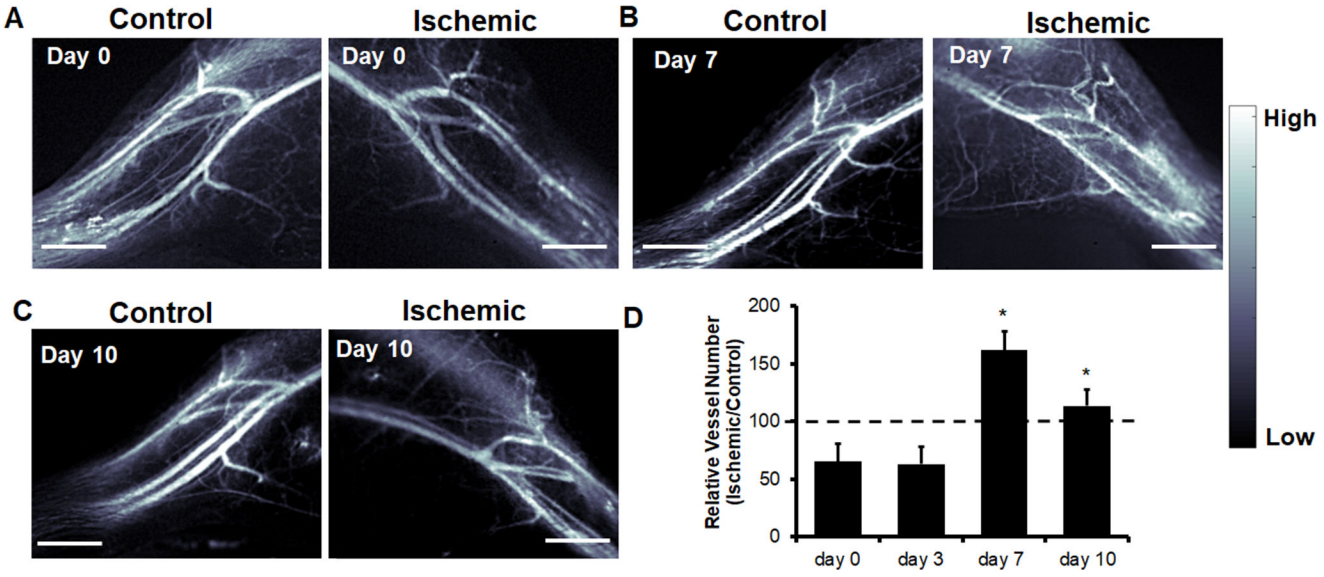

Figure 5.

High-magnification NIR-IIb fluorescence imaging of vascular regeneration in the ischemic hindlimb. A, B, C. Fluorescence images of mouse hindlimb vasculature on days 0, 7 and 10 after induction of hindlimb ischemia. Shown are the vasculature in the ischemic limb and control (unoperated) limb. D. Quantification of microvessel formation in the ischemic limb during revascularization (n>4). Scale bar: 2 mm. Statistically significant difference in comparison with day 0 is shown as *P<0.05